δ¹⁸O and salinity variability from the Last Glacial Maximum to Recent in the Bay of Bengal and Andaman Sea

A.V. Sijinkumar [a, b, *], Steven Clemens [a], B. Nagender Nath [b], Warren Prell [a], Rachid Benshila [c], Matthieu Lengaigne [d, e]

[a] Earth, Environmental, and Planetary Sciences, Brown University, Providence, RI, USA
[b] CSIR-National Institute of Oceanography, Dona Paula, Goa, India
[c] CNRS/LEGOS, Toulouse, France
[d] LOCEAN, IPSL, Sorbonne Universités (UPMC, Univ. Paris 06)/CNRS/IRD/MNHN, Paris, France
[e] Indo-French Cell for Water Sciences, IISc-NIO-IITM—IRD Joint International Laboratory, NIO, Goa, India

ABSTRACT

Oxygen isotopes of surface, thermocline and bottom dwelling foraminifera were analysed from two well-dated Andaman Sea cores and combined with nine previously published records from the Bay of Bengal (BoB) and Andaman Sea to create a transect spanning 20°N to 5°N. Combined with temperature estimates and the observed seawater δ¹⁸O-salinity relationship, these data are used to estimate past changes in BoB salinity structure. Compared to modern, mid-Holocene (9—6 cal ka BP) surface waters in the northern BoB were 2.5 psµ (8%) fresher, Andaman Sea were 3.8 psµ (12%) fresher, and southern BoB were 1.2 psµ (3.5%) fresher. Conversely, during the last glacial maximum (LGM), surface waters in the northern BoB were 2.9 psµ (9%) more saline while Andaman Sea were essentially unchanged and southern BoB were 1.7 psµ (4.9%) more saline compared to modern. The relative freshness of the Andaman during the last glacial maximum is likely the result of basin morphology during sea level low stand, resulting in reduced surface water mixing with the open BoB as well as shelf emergence, causing increased proximity of the core locations to river outflow. Sensitivity experiments using a regional ocean model indicate that the increased mid-Holocene north to south (20°N to 5°N) salinity gradient can be achieved with a ~50% increase in precipitation/runoff while the decreased glacial age gradient can be achieved with a ~50% reduction in precipitation/runoff. During the deglaciation, both surface and thermocline-dwelling species in the Andaman and northern BoB exhibit depleted δ¹⁸O within the Younger Dryas (YD), indicating colder and/or more saline conditions. None of the records from the southern BoB site have clear YD structure, possibly due to the combined effects of bioturbation and low sedimentation rates.

© 2016 Elsevier Ltd. All rights reserved.

1. Introduction

The north-eastern Indian Ocean is an important region for reconstructing changes related to monsoon precipitation and river runoff (Fig. 1). The major rivers of India, Bangladesh and Myanmar (Ganges-Brahmaputra, Irrawaddy and Salween) are largely fed by summer monsoon precipitation and glacial meltwater and are responsible for delivering the majority of sediments to the Bengal Fan and Andaman Sea (Colin et al., 1998; 1999). Annual runoff to the Bay of Bengal (BoB) is estimated to be 2950 km³ (Fekete et al., 2002; Sengupta et al., 2006) and contributes to the freshwater flux into the BoB in equal proportion with rainfall over the ocean north of 15°N (Chaitanya et al., 2014), strongly impacting the BoB salinity budget (Rashid et al., 2007; Akhil et al., 2014).

Direct precipitation (P) plus runoff (R) exceeds evaporation (E) throughout the annual cycle (P + R−E>0) leading to a strong low salinity cap in the northern BoB and Andaman Sea, with saltier waters in the southern BoB (Duplessy, 1982; Kudrass et al., 2001; Rashid et al., 2007). The resulting north to south surface salinity gradient, with lowest salinity values in the north and highest in the south, largely reflects regional changes fresh water input via precipitation and runoff in the northern BoB. The East Indian Coastal Current, a well-defined, seasonally reversing western boundary
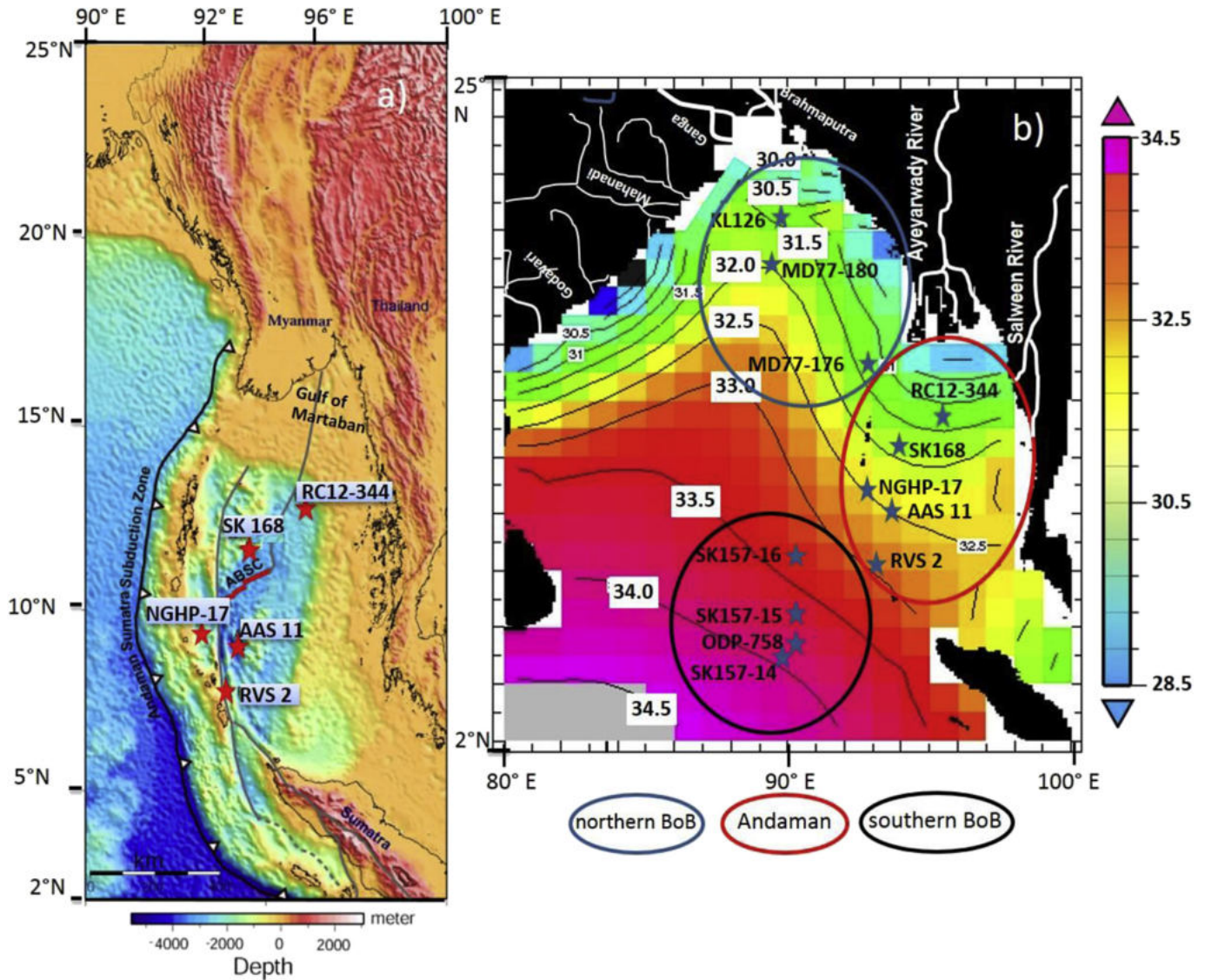
Fig. 1. Location map a) bathymetry of core locations in the Andaman Sea; b) Location of the sediment cores used in the BoB. Colour shading is the present day annual average surface salinity (data from Levitus and Boyer (1994)). (For interpretation of the references to colour in this figure legend, the reader is referred to the web version of this article.)

current in the BoB drives most of the exchange of water masses between the BoB and Arabian Sea (Akhil et al., 2014). Its southward flow right after the summer monsoon transports fresh waters from the northern BoB to the southern tip of India (Chaitanya et al., 2014). Its northward flow during southwest monsoon, which transports high-salinity water into the southernmost BoB from the Arabian Sea, subducts beneath the fresh, low-density surface waters at ~5°N such that the 35 psμ isohaline deepens to ~250 m depth by 15°N (Vinayachandran et al., 2013). Thus, the BoB surface salinity gradient is not impacted by mixing with Arabian Sea surface waters, but rather, by loss of fresh water to depth by vertical mixing (Akhil et al., 2014). The dominant response of the surface salinity gradient to insitu processes make it ideal for reconstructing changes in monsoon-driven precipitation and runoff.

Various workers have utilized deep sea sediments from the BoB and the Andaman Sea to study past monsoon variability (eg. Chen and Farrell, 1991; Cullen, 1981; Govil and Naidu, 2011; Kudrass et al., 2001; Rashid et al., 2007), changes in surface and deep water circulation (eg. Ahmad et al., 2008; Raza et al., 2014) as well as

sediment provenance and the tectonic history of source regions (eg. Ali et al., 2015; Awasthi et al., 2014; Colin et al., 1998; 1999; 2006; Kurian et al., 2008). Cullen (1981) first reconstructed BoB north-south salinity gradients using planktonic foraminiferal assemblage data. Cullen found higher glacial age salinity and a reduced north to south salinity gradient but no change in Holocene salinity relative to modern. These results were attributed to local changes in precipitation and runoff, having eliminated the impact of meltwater on the basis of volumetric estimates of modern ice mass and river discharge.

This study utilizes a suite of eleven AMS dated records spanning 20° N to 5°N, including BoB and Andaman Sea sites. We combine the $\delta^{18}O$ of surface-, thermocline- and botton-dwelling foraminifera with paired records of sea surface temperature (SST) to reconstruct changes in the BoB N-S salinity gradients during the LGM, when the summer monsoon is thought to be relatively weak and the early Holocene, when the summer monsoon is thought to be relatively strong (Cullen, 1981, Marzin et al., 2013; Govil and Naidu, 2011; Kudrass et al., 2001; Rashid et al., 2007).

The modern north to south salinity gradient in the BoB is reflected in the $\delta^{18}O$ of surface dwelling planktic foraminifera (*Globigerinoides ruber* and *Globigerinoides sacculifer*) preserved in the underlying sediments (Duplessy, 1982). Oxygen isotope records of *Globigerinoides ruber* and *Pulleniatina obliquiloculata* can be used to monitor changes in the mixed layer and thermocline structure resulting from changes in temperature and fresh water input (direct precipitation and river runoff) (Bolton et al., 2013; Mohtadi et al., 2011). *G. ruber* is a surface-dwelling species that lives throughout the year within the 0—50 m depth range (Anand et al., 2003). *P. obliquiloculata* is a species which lives in the subsurface waters responding to ambient conditions at the thermocline (Ravelo et al., 1990). In the Andaman Sea, the abundance of this species varies with changes in winter monsoon and thermocline depth (Sijinkumar et al., 2011). We used benthic species *Cibicidoides wuellerstorfi* to monitor the bottom water isotopic composition (Belanger et al., 1981) which largely reflects the global $\delta^{18}O$ variability associated with changes in terrestrial ice volume.

We generated benthic $\delta^{18}O$ (*C. wuellerstorfi*), planktic $\delta^{18}O$ (*P. obliquiloculata*) and planktic $\delta^{18}O$ (*G. ruber,* white) to monitor changes in the bottom, thermocline and mixed layer $\delta^{18}O$ at Andaman Sea sites SK 168 and RVS 2. Previously, Bolton et al. (2013) generated paired planktonic $\delta^{18}O$ data (*G. ruber* and *Neogloboquadrina dutertrei*) at ODP Site 758, making a total of three BoB sites with paired thermocline and mixed layer records (SK 168, RVS 2 and ODP 758). We compile and analyze these along with eight other *G. ruber* records and seven other benthic (*C. wuellerstorfi*) records from the literature in an effort to better reconstruct changes in deep, thermocline and mixed-layer structure. In total, the *G. ruber* records span 5°N to 20°N, creating a transect along the entire length of the BoB (Fig. 1). The three paired mixed layer and thermocline records span 5°N to 12°N. Benthic records span a very similar range (5°N to 13°N). We analyze this eleven site $\delta^{18}O$ transect (5—20°N), utilizing existing, but sparse, temperature data (KL 126, RC 12-344 and ODP 758) and the modern BoB surface water $\delta^{18}O$—salinity relationship to estimate changes in basin-wide salinity at the LGM and mid-Holocene. We finally perform sensitivity experiments using a regional configuration of the NEMO ocean model in the BoB (Benshila et al., 2014) to estimate the changes in precipitation and runoff necessary to replicate the observed gradients.

2. Oceanographic setting

2.1. Modern oceanography and climatology

The BoB is characterized by seasonal monsoon circulation patterns and large fresh water discharge from the Ganges-Brahmaputra, Irrawaddy and Salween river basins. As a result, salinity decreases during the summer monsoon (July to August), reaching a minimum in September and October due to the delayed influence of river runoff (Fig. 2c).

The annual average salinity at the northernmost core location (~20°N; KL 126) is ~30 psµ while salinity at the southernmost core location (~5°N; SK157-14) is 3.8 psµ higher (Table 1). This north to south gradient within the BoB (~0.2 psµ/latitude) is roughly similar to that found in the Andaman Sea (~0.3 psµ/latitude), the difference likely due to isolation of the Andaman surface waters by the Andaman-Nicobar arc and associated islands (Benshila et al., 2014).

Seasonal SST variability in the BoB is very small with the lowest values (~26 °C) in the north during winter and ~28—29 °C basin-wide throughout summer (Locarnini et al., 2010). The annual surface water temperature in the Andaman Sea ranges from 28 to 30 °C

and is nearly homogenous up to a depth of 50 m (Sarma and Narvekar, 2001). The combined thermal and fresh water forcing leads to strong stratification in both the Andaman and BoB (Fig. 2a), which hinders vertical mixing (Thadathil et al., 2007), eventually impacting regional climate (Shenoi et al., 2002), primary productivity (Gauns et al., 2005; Prasanna Kumar et al., 2002) and tropical cyclone intensity (Neetu et al., 2012).

Intermediate to deep water circulation between the BoB and the Andaman Sea is limited due to the presence of sills, including Deep Prepares Channel, Ten Degree Channel, and the Great Channel (Fig. 1a). Above these sill depths, water column structure (temperature and salinity) in the Andaman and open BoB is comparable (to a depth of 1300 m) but diverge at greater depths (Fig. 2a, b) (Naqvi et al., 1994). The deep waters of the Andaman Sea are warmer, less saline, and have lower dissolved oxygen than BoB waters of comparable depth (Fig. 2a, b).

2.2. Modern BoB $\delta^{18}O_{sw}$ -salinity relationship

The spatial $\delta^{18}O_{sw}$-salinity relationship is linear in the global oceanic surface water with a slope of ~0.38‰/psu ($n = 22,934$, $R^2 = 0.80$) (Schmidt et al., 1999). In the BoB, strong river runoff and dominance of precipitation over evaporation results in a significantly lower $\delta^{18}O_{sw}$-salinity slope (Delaygue et al., 2001). The strong BoB salinity gradient is reflected in $\delta^{18}O_{sw}$ with lowest values in the north and highest values in the south. The BoB $\delta^{18}O_{sw}$-salinity relationship varies with season and geographic location, increasing with evaporation and decreasing with increased runoff and precipitation (Achyuthan et al., 2013; Delaygue et al., 2001; Singh et al., 2010).

We have synthesized all available paired $\delta^{18}O_{sw}$-salinity data from the BoB in order to establish a relationship representing the largest geographical and seasonal coverage possible (Fig. 2d). This synthesis includes data from Schmidt et al. (1999) supplemented with recently published data from Sengupta et al. (2013) and Achyuthan et al. (2013). Despite a large number of data points ($n = 406$) there remains a deficit of data for May ($n = 14$), June ($n = 5$) and October ($n = 0$) as well as a bias toward data collected in the western half of the basin (80—90°E). The compiled BoB records yield a $\delta^{18}O_{sw}$-salinity slope of 0.15‰/psu ($\delta^{18}O = 0.15$, psu - 4.91; $n = 406$, $r^2 = 0.39$) (Fig. 2d). To assess for spatial and seasonal bias, we calculated the slope using a 2° latitudinal average spanning 5° to 23°N (0.18‰/psu; $n = 9$, $r^2 = 0.89$) and a monthly average (0.13‰/psu; $n = 12$, $r^2 = 0.46$).

For this work, we use the 0.15‰/psu slope derived from the full BoB data set. This slope is consistent with that from box model stimulations of Delaygue et al. (2001) for model points with river runoff included (0.14‰/psu); for comparison, the slope for model points without runoff is over twice as large, equivalent with the global slope. The use of the 0.15‰/psu slope is also consistent with the more rigorous treatment of the Schmidt et al. (1999) data set by LeGrande and Schmidt (2006). They calculated a slope of 0.16‰/psu for the entire Indian Ocean. Given the uniquely strong rainfall and runoff regime in the BoB, the 0.15‰/psu slope is significantly less than that of the Pacific and Atlantic over the same latitude range (0.37‰/psu).

We apply this $\delta^{18}O_{sw}$-salinity relationship to both mid-Holocene and LGM data to estimate changes in BoB salinity, assuming that the relationship is stable across these regimes. This assumption has been employed previously for Holocene reconstructions (Leduc et al., 2013). We do so as well for the LGM, citing the Delaygue et al. (2001) modelling results which indicate limited change in the LGM BoB slope, with consequent limited error on resulting paleosalinity estimates.
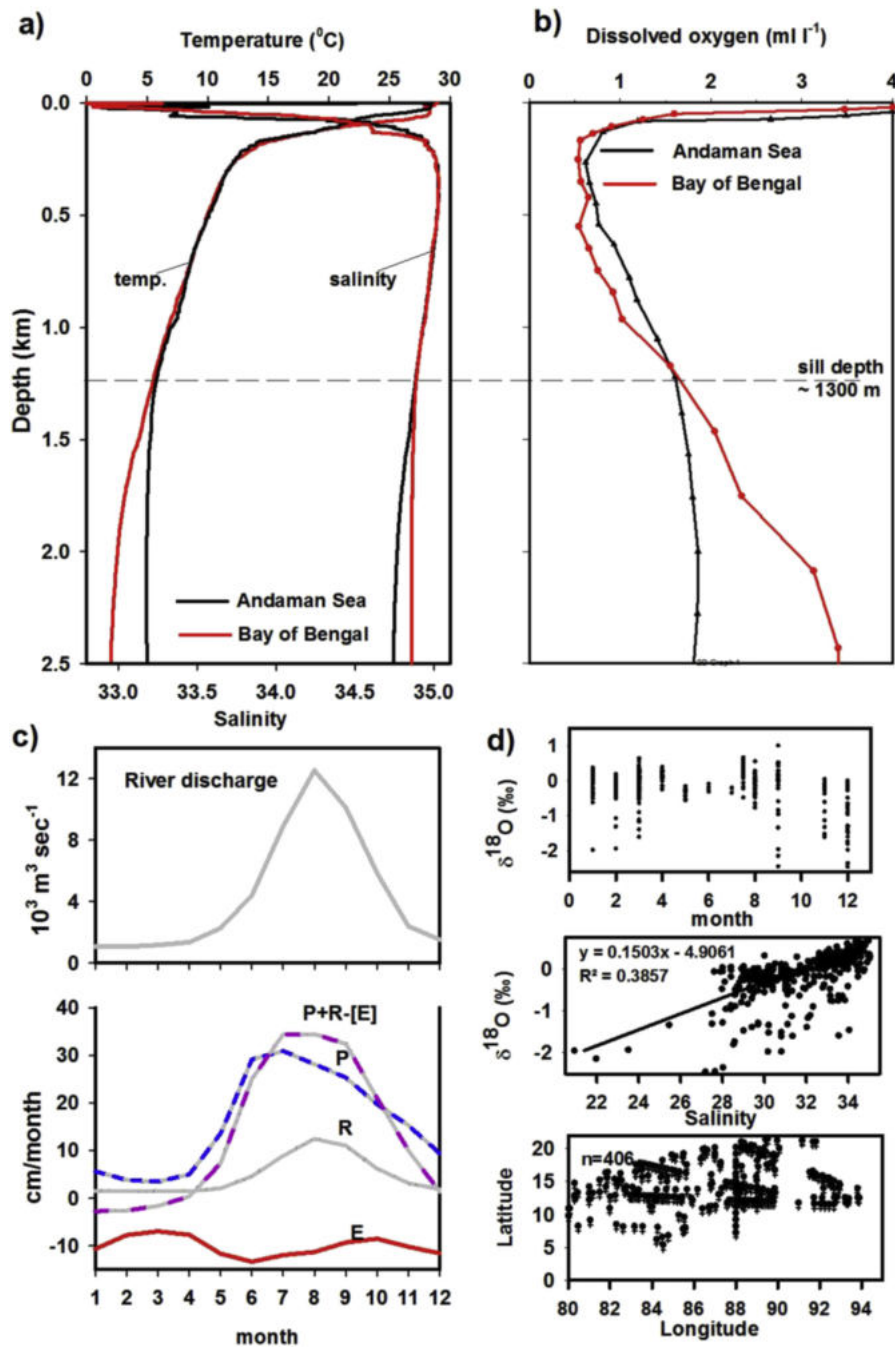
Fig. 2. a) Vertical profiles of temperature and salinity at two representative CTD stations in the Andaman Sea (10.25 N/94.078 E) and the Bay of Bengal (12.15 N/91.415 E); b) dissolved oxygen data from the BoB and the Andaman Sea (Naqvi et al., 1994); c) Average annual cycle of river discharge from the major rivers (Ayeyarwady, Ganges, Brahmaputra, Mahanadi, Godavari, Krishna and Cauvery) (Data source: http://www.sage.wisc.edu/riverdata/) and annual cycle of evaporation (E), river discharge (R), precipitation (P), P + R-(E) in the BoB (Rao and Sivakumar, 2003); d) δ^{18}O sea water data versus month, surface δ^{18}O-salinity relationship for the BoB (Achyuthan et al., 2013; Schmidt et al., 1999; Sengupta et al., 2013) and spatial distribution of sampling sites in the BoB (latitude versus longitude).

3. Materials and methods

3.1. Sediment cores

The sediment cores SK 168 (water depth: 2064 m) and RVS 2 (water depth: 2301 m) were collected from the Andaman Sea (Fig. 1). The locations of the new records presented here and those compiled from existing literature are listed in Table 1. SK 168 was collected during the 168th cruise of ORV Sagar Kanya from the Alcock Seamount Complex in the Andaman Sea. Core RVS 2 was

collected during the Indian Ridge expedition onboard German Research vessel F. S. Sonne.

3.2. Planktic and benthic δ^{18}O analyses

Approximately 20 tests of *P. obliquiloculata* in the size range of 250−315 µm were picked, cleaned, and homogenised by grinding with ethanol. A sub-fraction (~40 µg) was used for oxygen isotope analysis. For benthic foraminifer, two to three specimens of the *C. wuellerstorfi* were used for δ^{18}O analysis. *P. obliquiloculata* and

Table 1
North to South δ^{18}O and estimated salinity.

Sl. No.	Core	Latitude (°N)	Longitude (°E)	Recent δ^{18}O (‰)[a]	Mid-Holocene δ^{18}O (‰)[a]	LGM δ^{18}O (‰)[a]	N to S mid-Holocene δ^{18}O difference (‰)[b]	N to S mid-Holocene temperature difference (°C)[d]	N to S mid-Holocene salinity difference (psu)[c]	Recent minus LGM δ^{18}O (‰)	Modern annual average salinity (psu)[f]	Mid-Holocene salinity[e]	Propagated salinity error[h]	LGM salinity [g]	Propagated salinity error[h]
1	KL126	19.9733	90.0338	−3.00	−3.4	−1.07	−0.99	−0.92	−5.1	−1.93	30.11	27.87	1.8	33.76	1.9
2	MD77-180	18.4675	89.4167	−2.80	−2.98	−0.91	−0.57	−0.83	−2.4	−1.89	31.16	30.52	1.7	34.54	1.9
3	MD77-176	14.5014	93.1183	−3.08	−3.42	−1.46	−1.01	−0.58	−5.8	−1.62	31.85	27.17	1.8	33.43	1.8
4	RC12-344	12.4600	96.0400	−3.29	−3.26	−1.35	−0.85	−1.00	−4.0	−1.94	31.82	28.94	2.2	32.03	2.4
5	SK168	11.4246	94.2961	−3.02	−3.44	−1.21	−1.03	−0.86	−5.4	−1.81	32.49	27.50	2.2	31.84	2.3
6	AAS 11	9.0000	94.2833	−3.20	−3.12	−1.44	−0.71	−0.52	−3.9	−1.76	33.04	29.08	2.2	32.05	2.3
7	RVS 2	7.4250	93.5800	−2.78	−2.99	−0.75	−0.58	−0.31	−3.4	−2.03	33.27	29.59	2.2	34.08	2.4
8	SK157-16	7.8000	90.8333	−2.34	−2.46	−0.62	−0.05	−0.14	−0.1	−1.72	33.56	32.84	2.5	36.12	2.6
9	SK157-15	8.7667	90.3000	−2.21	−2.54	−0.7	−0.13	−0.22	−0.5	−1.51	33.52	32.44	2.5	34.69	2.6
10	ODP758	5.3841	90.3945	−2.42	−2.58	−0.78	−0.17	−0.01	−1.1	−1.64	33.84	31.83	2.5	35.86	2.6
11	SK157-14	5.1833	90.0833	−2.40	−2.41	−0.93	0.00	0.00	0.0	−1.47	33.94	32.94	2.5	34.82	2.6

[a] *G. ruber*: Recent (2−0 ka; MD77-180 extrapolated on the basis of nearby KL126); Mid-Holocene average (9−6 ka), LGM average (23−19 ka).

[b] *G ruber* δ^{18}O value for each core minus −2.41 (value at southernmost core SK157-14).

[c] North to south Mid-Holocene δ^{18}O difference minus north to south Mid-Holocene temperature difference (converted to ‰ using 0.25‰/°C) then converted to salinity by dividing by the 0.15‰/psu BoB relationship.

[d] North to south temperature gradient. Gradient for the BoB sites derived from KL126 (27.24 °C) and ODP 758 (28.16 °C) then linearly interpolated as a function of latitude. Gradient for the Andaman sites derived from RC12-344 (27.16 °C) and ODP758 (28.16 °C) then linearly interpolated as a function of latitude.

[e] 32.94 psu plus the N to S mid Holocene salinity difference. 32.94 is the mid-Holocene salinity value at SK1567-14, estimated to be 1 psu less than the modern value on the basis of the measured 0.15‰ mid-Holocene to core-top difference at high-resolution ODP758 (0.15‰ divided by 0.15‰/psu = 1 psu).

[f] World Ocean Atlas (Antonov et al., 2010).

[g] Recent minus LGM δ^{18}O value corrected for global ice volume (1.2‰) and SST (LGM minus Recent) converted to ‰ using 0.25‰/°C. The temperature correction for northern BoB cores is from KL126 (27.07−27.8 = −0.73 °C; Kudrass et al. (2001)); The temperature correction applied to Andaman cores is from RC12-344, 25.57−28.4 = −2.83 °C, Rashid et al. (2007), The temperature correction applied to southern BoB cores is from ODP 758 (27.48−28.03 = -0.55 °C; (Chen, 1994).

[h] Error propagation for the paleosalinity estimates includes analytical error for δ^{18}O (0.06‰), SST (Mg/Ca at ±1 °C, Alkenone at ±1.3 °C and foraminifera modern analog technique at ±1.5 °C, Schmidt (1999)) and the δ$^{18}O_{sw}$-salinity slope regression (0.009).

C. wuellerstorfi samples were analysed at the Department of Earth, Environment and Planetary Sciences, Brown University, on a Finnigan MAT 252 dual-inlet isotope ratio mass spectrometer with a Kiel III carbonate device. Isotopic compositions are reported in δ notation as per mil deviation from VPDB standard; analytical precision was better than 0.06‰ (1σ). For core SK 168, $\delta^{18}O$ *G. ruber* and *P. obliquiloculata* were analysed from a total 125 samples while 85 samples were analysed for *C. wuellerstorfi* (due to insufficient specimens at some depths). *C. wuellerstorfi* $\delta^{18}O$ values of core SK 168 were adjusted by adding 0.64‰ to make them consistent with those from *Uvigerina* spp. measured on other cores (Shackleton and Hall, 1984); similar corrections are also applied to other published records as necessary (NGHP-17 and RC 12-344).

3.3. Age model

Age models for all records have been previously published, largely based on Accelerator Mass Spectrometer (AMS) ^{14}C dates of planktic foraminiferal tests, and are summarized in Fig. 3. We accept these age models as published with no modifications. All records span the past 25 ka with the majority spanning the past 55 ka. Average temporal resolution varies between 0.115 and 2.2 kyrs. New data presented here from cores SK 168 and RVS 2 are resolved at 0.43 kyrs per sample. The accuracy of the age model of core SK 168 and RVS 2 is supported by comparison to the ODP 758 oxygen isotope record (Bolton et al., 2013) and global benthic stack (Lisiecki and Raymo, 2005) (Fig. 4). The last glacial to Holocene sedimentation rates for these sites range widely from 2.2 to 30 cm/ka; the higher sedimentation rate cores are located in the northern BoB and Andaman Sea (Fig. 3). The average sedimentation rate for cores SK 168 and RVS 2 during last glacial to Holocene are 8 and 21 cm/ka respectively.
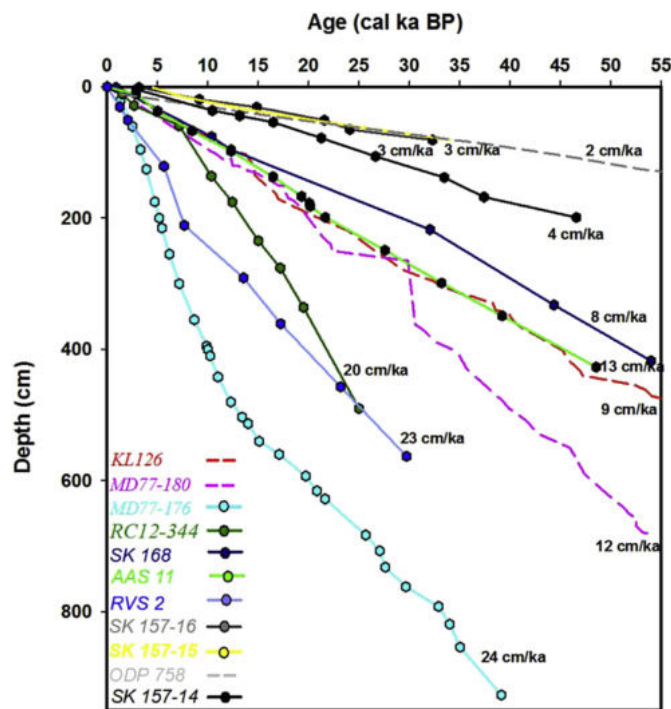
Fig. 3. Age model summary for all records, largely based on Accelerator Mass Spectrometer (AMS) ^{14}C dates of planktic foraminiferal tests (continuous line with symbols) and oxygen isotope stratigraphy (broken lines, cores KL 126, MD 77-180 and ODP 758).

3.4. Error propagation

Error propagation for the paleosalinity estimates follow Schmidt (1999) and includes analytical error for $\delta^{18}O$ (0.06‰), SST, and the $\delta^{18}O_{sw}$-salinity slope regression (0.009). Our paleosalinity error estimates are dominated by error in the paleotemperature estimates; following Schmidt (1999) we assigned errors for Mg/Ca at ±1 °C, Alkenone at ±1.3 °C and foraminifera modern analog technique at ±1.5 °C (Table 1).

3.5. Model simulations

We use a regional ocean model configured for the BoB to assess the change in freshwater fluxes required to drive the observed salinity changes during mid-Holocene and LGM. The NEMO (Nucleus for European Modelling of the Ocean) model (Madec, 2008) is described in detail in Benshila et al. (2014). Vertical mixing is parameterized with a prognostic turbulent kinetic energy scheme, with background vertical diffusion and viscosity of 10^{-5} m^2 s^{-1} and 10^{-4} m^2 s^{-1}, respectively. The vertical grid has 75 vertical levels, increasing from 1 m at the surface to 250 m at depth. The horizontal grid is based on a Mercator projection at ¼° resolution, allowing capture, to a certain extent, of oceanic mesoscale features such as oceanic eddies. The geographic domain of the model spans the entire BoB, from 2.25°N to 22.8°N, 77.3°E to 100°E. The southern, eastern and western boundaries are open, treated with a radiation-relaxation approach (Marchesiello et al., 2001), and constrained with a 150 day time-scale relaxation to the monthly velocities, temperature and salinity of an interannual global ¼°simulation performed at Mercator-Ocean.

The control simulation, referred as CTL in the following, is forced with the interannual hybrid DRAKKAR Forcing Set 5 (Dussin et al., 2014) that computes fluxes using bulk formulae from ERA-interim (Dee et al., 2011) turbulent variables (wind, humidity and air temperature) and satellite data for radiation (Zhang et al., 2004). The freshwater flux injected into the BoB combines the oceanic precipitation from the GPCP product (Huffman et al., 2001) and Ganges-Brahmaputra and Irrawaddy runoff derived from satellite altimetry, as described in Papa et al. (2012). No surface salinity restoring is performed. Experiments using this model configuration and a similar forcing strategy have been shown to successfully reproduce the modern seasonal sea surface salinity variability in the BoB (Benshila et al., 2014). Each of the CTL and sensitivity experiments (introduced below) is run over the 1999−2008 period after a 6 year spin-up.

We perform a series of sensitivity experiments, differing only from CTL experiment by the amount of freshwater injected into the BoB. A simple multiplicative factor α is applied to both oceanic rainfall and river runoff to assess the modeled salinity sensitivity to freshwater flux amount. We perform four such sensitivity experiments, α being 0, 0.5, 1.5 and 2, referred to in the following as CTLx0, CTLx0.5, CTLx1.5 and CTLx2 respectively. These experiments alter only fresh water flux and do not incorporate changes in climatological boundary conditions (e.g. winds, radiation, ice-volume) known to exist during the LGM and mid-Holocene.

4. Results

The oxygen isotope records of surface, thermocline and bottom dwelling species for SK168, RVS2 (this work) and ODP 758 (Bolton et al., 2013) are presented in Figs. 4 and 5. AMS-dated sample depths are also marked in Fig. 4. Northern (SK 168) and southern (RVS 2) Andaman Sea $\delta^{18}O$ *G. ruber* values are offset by an average of 0.4‰ over the length of the records, although the values converge during the YD (Fig. 4). In contrast, the $\delta^{18}O$ *P. obliquiloculata* values
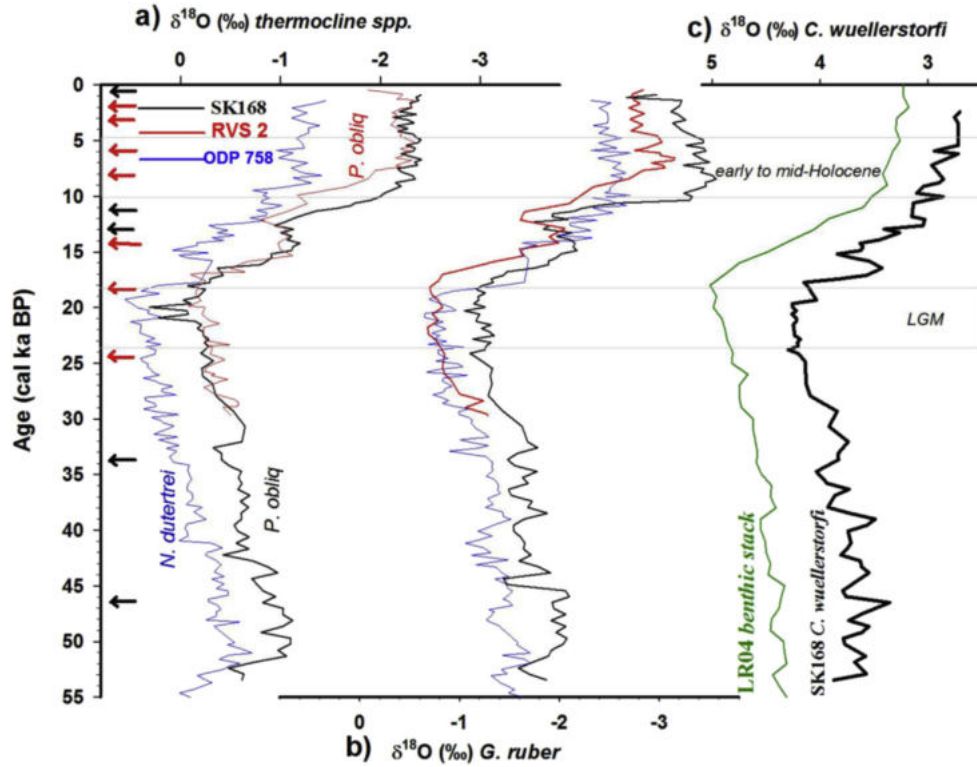
Fig. 4. Paired surface and thermocline δ18O records and benthic δ18O for SK168 a) δ18O record of thermocline spp., viz. *P. obliquiloculata* (core SK 168 and RVS 2) and *Neogloboquadrina dutertrei* (core ODP 758; Bolton et al. (2013)); b) δ18O *G. ruber* for the cores SK 168, RVS 2 (Sijinkumar et al., 2015) and ODP 758; c) δ18O*C. wuellerstorfi* of core SK 168 with LR04 benthic record (Lisiecki and Raymo, 2005). Arrow marks represent AMS 14C dated horizons.
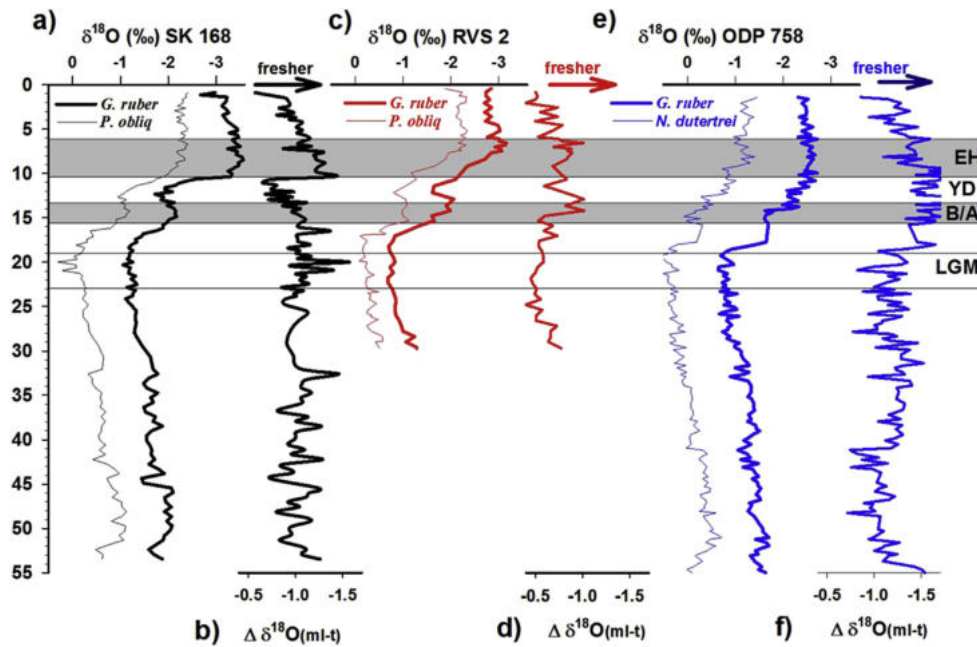
Fig. 5. Mixed-layer to thermocline δ18O differences as a proxy for freshening a) δ18O_obliq and δ18O_ruber of core SK 168; b) The record Δδ18O G. ruber (mixed layer) minus P. obliquiloculata (thermocline; Δδ18O_(ml−t)) of core SK 168; c) δ18O_obliq and δ18O_ruber of core RVS 2; d) The record Δδ18O G. ruber minus P. obliquiloculata (Δδ18O_(ml−t)) of core RVS 2; e) δ18O_obliq and δ18O_ruber of core ODP 758; f) The Δδ18O_(ml−t) of core ODP 758 (Bolton et al., 2013).

from these two Andaman Sea locations show no systematic north to south offset. Fig. 5 illustrates that, over the long term (LGM to Recent), the paired deep- and shallow-dwelling δ18O records exhibit similar changes in both timing and amplitude at each of the

three individual sites. During the deglaciation, both surface and thermocline-dwelling species in the Andaman exhibit depleted δ18O within the Younger Dryas (YD) relative to the Bolling-Allerod (B/A) and early Holocene. Neither the δ18O *G. ruber* nor the δ18O

N. dutertrei records at the southern BoB site (ODP 758) indicate clear deglacial-age YD structure.

The SK 168 benthic ($\delta^{18}O_{wue}$) record (Fig. 4c) is distinctly different from the paired planktonic record in that it lacks clear deglacial B/A and YD structure, as is commonly the case with benthic $\delta^{18}O$ records (Figs. 6 and 7). The benthic $\delta^{18}O$ LGM to mid-Holocene amplitude is 1.2‰ whereas the *G. ruber* LGM to mid-Holocene difference is much larger (2.2‰). These relationships are also evident in northern Andaman Sea core RC12-344 (Figs. 6 and 7) but not seen in the other paired benthic and planktonic records to the south. The $\delta^{18}O$ mixed layer minus $\delta^{18}O$ thermocline ($\Delta\delta^{18}O_{(ml-t)}$) provides an indication of surface water warming or freshening (Bolton et al., 2013). $\Delta\delta^{18}O_{(ml-t)}$ values for the BoB are shown in Fig. 5. Depleted values occur during the mid-Holocene followed by more enriched values during the late Holocene in all three cores. Enriched $\Delta\delta^{18}O_{(ml-t)}$ values are also seen during YD at both Andaman locations but not at ODP 758.

The $\delta^{18}O_{ruber}$ and $\delta^{18}O_{wue}$ of all cores (20°−5°N) are shown in Figs. 6 and 7. The $\delta^{18}O_{wue}$ records exhibit LGM (23−19 ka average) to Holocene (10−0 ka average) amplitudes ranging from 1.24 to 1.59‰ with the largest amplitudes being found furthest south (ODP 758 and SK 157-14). Mean $\delta^{18}O_{wue}$ values for the Andaman sites (0−30 ka) are ~1.25‰ lighter compared to southern BoB sites, consistent with warmer and fresher Andaman deep waters (Fig. 2a, b). Fig. 8 shows the $\delta^{18}O$ gradient between LGM and mid-Holocene for mixed layer, thermocline and benthic species.

All the $\delta^{18}O_{ruber}$ records indicate nearly the same heaviest LGM values (-0.77 ± 0.17‰) while the lightest Holocene values vary significantly from -3.84 in the northern BoB (MD 77-176) to -2.57‰ in the south (SK 157-15) (Fig. 6). Larger amplitude and more abrupt glacial to Holocene transitions are observed in the northern compared to the southern $\delta^{18}O_{ruber}$ records (Fig. 6). North to south differences between mid-Holocene and Recent values at each site are also evident (Table 1). Larger average differences (mid-Holocene minus Recent) are found in the northern BoB (-0.31‰) compared to the Andaman (-0.13‰) and southern BoB (-0.15‰) regions.

Modelling results illustrate the change in fresh water input (precipitation and runoff) required to achieve the reconstructed salinity estimates (Fig. 10; Tables 1 and 2). The modeled modern BoB north to south salinity gradient (3.5 psμ) is similar to that derived from modern climatology (3.8 psμ). Similarly, the modeled gradient for the CTLx1.5 experiment (5.09 psμ) matches the proxy estimated mid-Holocene gradient (5.07 psμ). Finally, the modeled gradient for the CTLx0.5 experiment (1.17 psμ) matches the LGM proxy estimated gradient (1.06 psμ) (Table 2).

5. Discussion

The BoB is the core convective region of the Indian monsoon system and arguably among the most seasonally impacted of all monsoonal regions (by direct summer monsoon precipitation and runoff from the surrounding catchment basins). Analysis of the surface water $\delta^{18}O$ signal through time provides a means of documenting spatial and temporal changes in this system. Andaman Sea records play a key role in reconstructing changes in the north to south (20°N to 5°N) surface water structure. Andaman Sea bathymetry provides coring sites at sufficiently shallow depths, yielding good carbonate preservation, and continuous sedimentation. These conditions are difficult to meet at the same latitudes in the central BoB, characterized by poor carbonate preservation and turbidite deposition, and in the Krishna-Godavari basin on the eastern Indian margin, which is heavily faulted and slumped (Ramprasad et al., 2011). The modern BoB salinity gradient (Tables 1 and 2) illustrates that the four Andaman records fit well into the eleven site transect, having higher salinity values on average compared to records from the northern BoB and lower salinity values on average compared to records from the southern BoB. Combining our new data sets generated from the Andaman Sea with existing data, we are able to reconstruct meridional changes in surface waters from the LGM to Recent, focusing on the mid-Holocene and LGM intervals.

5.1. LGM, mid-Holocene and Recent $\delta^{18}O$ and salinity estimates

5.1.1. LGM compared to mid-Holocene $\delta^{18}O$
5.1.1.1. *Records with paired benthic and planktonic $\delta^{18}O$.* Comparison of records with both benthic and planktonic $\delta^{18}O$ suggests large changes in the LGM to mid-Holocene meridional surface water $\delta^{18}O$ structure in the BoB. The deglacial amplitude (LGM to mid-Holocene) for Andaman and southern BoB benthic records combined have a narrow range (1.38 ± 0.16‰, $n = 6$). In contrast, the deglacial amplitude of the planktonic records systematically increases from 1.49‰ in the southernmost BoB (SK157-
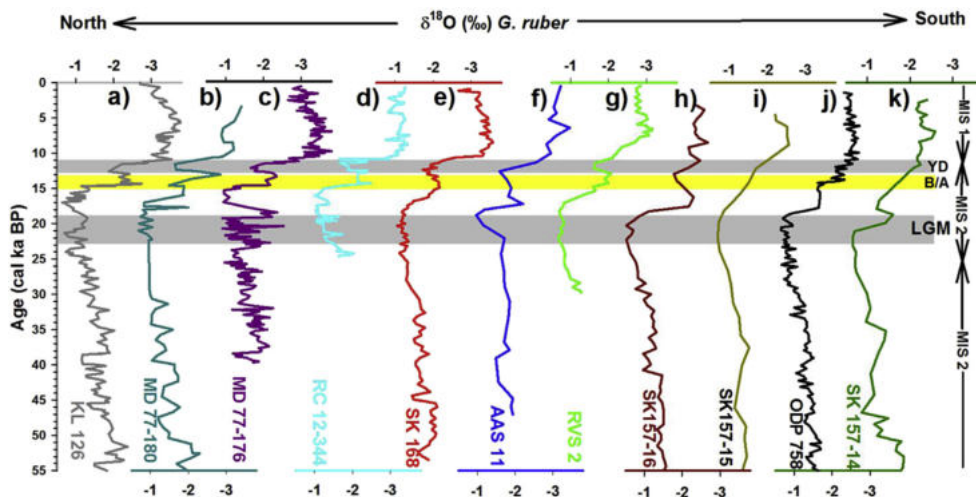
Fig. 6. G. ruber (mixed layer) oxygen isotope records a) core KL 126 (Kudrass et al., 2001); b) core MD 77-180 (Duplessy, 1996; Colin et al., 1998); c) MD77-176 (Marzin et al., 2013); d) RC 12-344 (Rashid et al., 2007); e) SK 168 (Sijinkumar et al., 2010) f) AAS 11 (Ahmad et al., 2000); g) RVS 2 (Sijinkumar et al., 2015) h) SK157-16 (Raza et al., 2014); i) SK 157-15 (Raza et al., 2014); j) ODP 758 (Bolton et al., 2013); k) SK 157-14 (Ahmad et al., 2008).
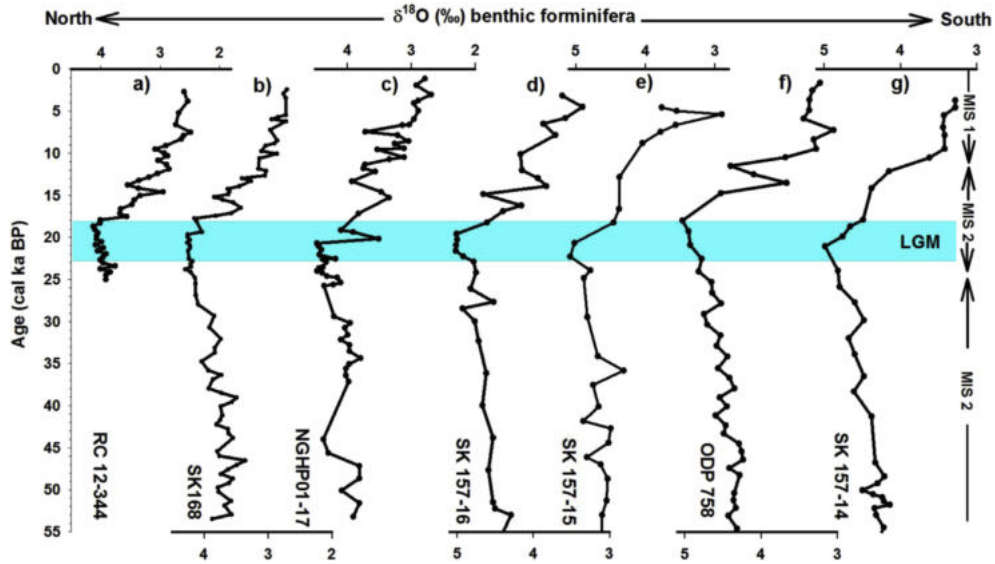
Fig. 7. Benthic oxygen isotope records. a) RC 12-344 (Naqvi et al., 1994); b) core SK 168; c) NGHP-17 (Ali et al., 2015); d) SK157-16 (Raza et al., 2014); e) SK 157-15 (Raza et al., 2014); f) ODP 758 (Bolton et al., 2013); g) SK 157-14 (Ahmad et al., 2008).
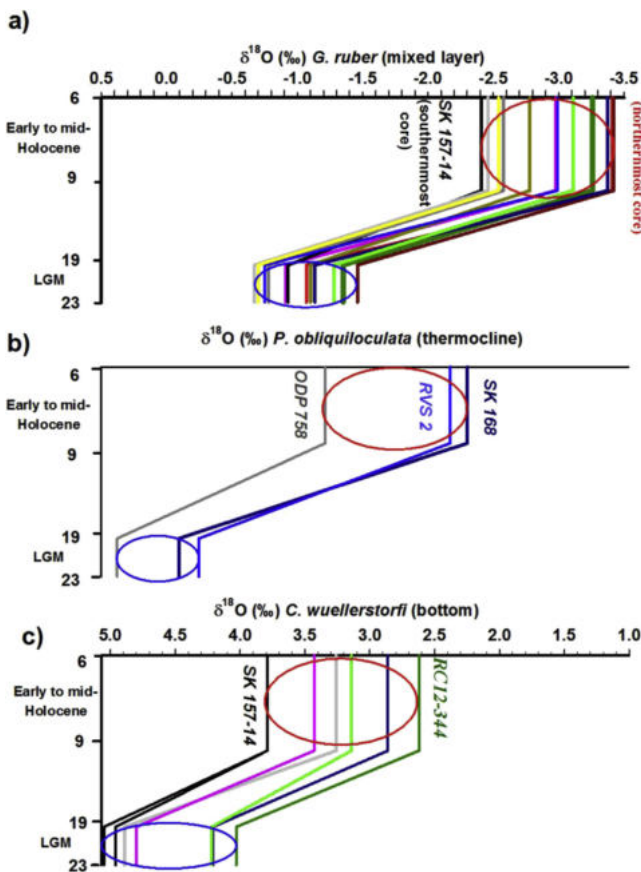
Fig. 8. Schematic representation of the LGM to mid-Holocene differences in $\delta^{18}O$ surface, thermocline and bottom waters in the N-S transect a) Surface water $\delta^{18}O$ (*G. ruber*; 20° N to 5°N); b) Thermocline $\delta^{18}O$ (*P. obliquiloculata* for core SK 168 and RVS 2 and *N. dutertrei* for core ODP 758 (12°N to 5°N); c) Bottom water $\delta^{18}O$ (*C. wuellerstorfi* (13°N to 5°N).

14) to 2.1‰ in the Andaman (average of SK 168 and RC 12-344). This indicates LGM to mid-Holocene freshening and/or warming of Andaman surface waters relative to southern BoB waters. This is consistent with the northern location of Irrawaddy and Salween outflow and a north to south mixing gradient (Fig. 1).

5.1.1.2. Records with paired mixed-layer and thermocline $\delta^{18}O$. Analysis of the two Andaman Sea records with paired mixed layer and thermocline $\delta^{18}O$ data (SK 168 and RVS 2) further constrains LGM to mid-Holocene $\delta^{18}O$ variability to the mixed-layer waters as follows. The $\delta^{18}O_{ruber}$ data, averaged over the common length of the records, show that the northern core (SK 168) is lighter by 0.4‰ (Fig. 4b) whereas the $\delta^{18}O_{obliq}$ data show no difference (Fig. 4a). This indicates similar temperature and salinity structure at thermocline depths but warmer and/or fresher mixed-layer waters to the north. To the extent that more northerly waters are generally cooler, this points to fresher mixed layer waters in the north, again consistent with proximity to Irrawaddy and Salween outflow (Fig. 1).

5.1.1.3. Records with mixed layer $\delta^{18}O$. Examination of all eleven $\delta^{18}O_{ruber}$ records allows expansion of our analysis into the northern BoB region. Similar LGM $\delta^{18}O_{ruber}$ maxima of all eleven records (−0.77 ± 0.17‰) but systematically depleted mid-Holocene values from south to north indicate progressively warmer and/or fresher waters to the north during the LGM to mid-Holocene transition. This results corroborate earlier reports of significantly enhanced of summer monsoon precipitation during the early Holocene (Marzin et al., 2013; Govil and Naidu, 2011; Kudrass et al., 2001; Rashid et al., 2007).

5.1.2. Mid-Holocene compared to recent $\delta^{18}O$

5.1.2.1. Records with paired mixed-layer and thermocline $\delta^{18}O$. All three records with paired mixed-layer and thermocline $\delta^{18}O$ show the same trend toward enriched $\Delta\delta^{18}O_{(ml-t)}$ values from the mid-Holocene toward the Recent, indicating increasing salinity or cooling of the mixed layer waters relative to thermocline waters.

5.1.2.2. Records with mixed layer $\delta^{18}O$. The average difference between mid-Holocene and Recent $\delta^{18}O_{ruber}$ values for northern BoB records is −0.31‰ whereas the differences for Andaman and southern BoB cores are −0.13‰ and −0.15‰ respectively. This indicates increasing salinity and/or cooling of mixed layer waters
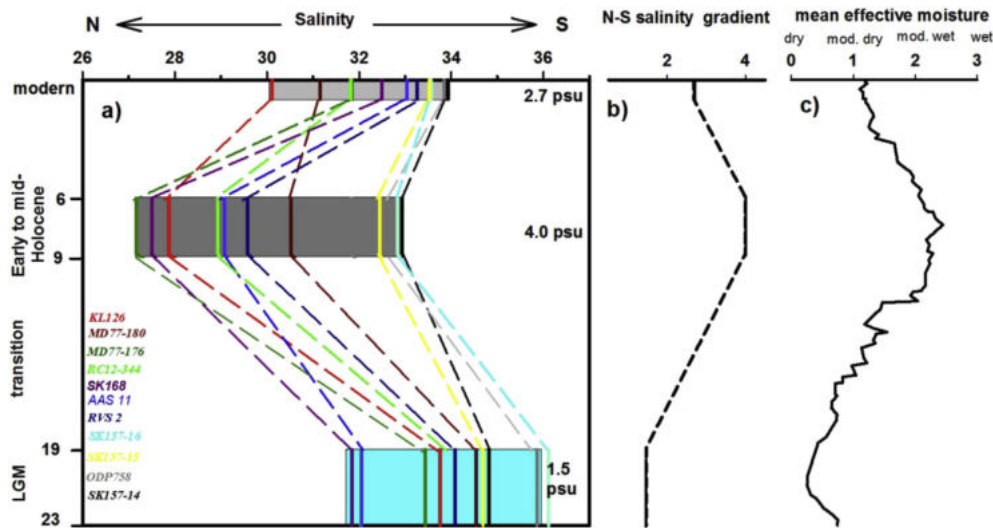
Fig. 9. Spatial and temporal changes in salinity and N-S salinity gradient a) Changes in salinity and N-S gradient during present, mid-Holocene and LGM. Shaded box represent the time domain over which salinity is reconstructed, the N-S gradient is marked on the right side. Modern salinity data from Antonov et al. (2010). Details of salinity reconstruction during mid-Holocene and LGM are presented in Table 1; b) N-S salinity gradient during LGM, early to mid-Holocene and modern between 5°N and 20°N; c) record of mean effective moisture evolution of Central Asia (Herzschuh, 2006).
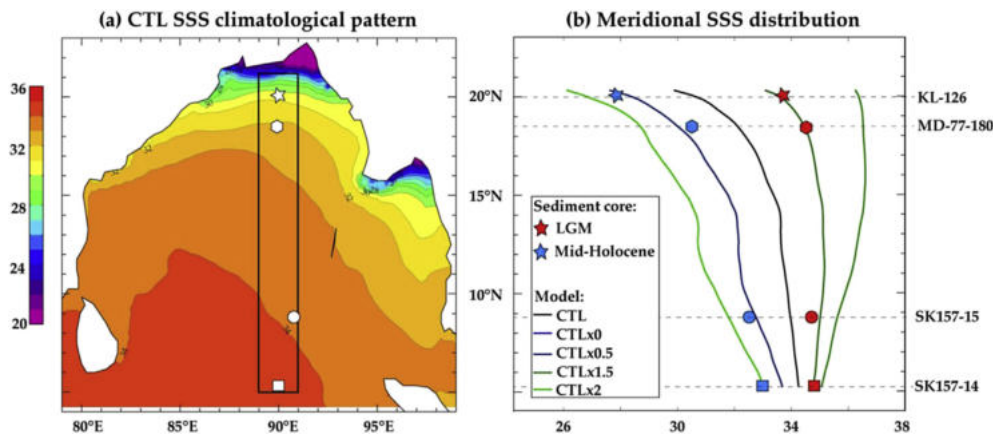
Fig. 10. Model freshwater sensitivity experiments a) CTL sea surface salinity with 90°E meridional transect outlined; b) Meridional sea surface salinity transects averaged between 89°E and 91°E (black frame on panel a) for CTL and sensitivity experiments where a constant coefficient α is applied to the total fresh water forcing (α; CTLx0, CTLx0.5, CTLx1.5 and CTLx2). Proxy sea surface salinity estimates from sediment cores in the northern and southern BoB (indicated by symbols on panels a) are also reported for mid-Holocene and LGM climate on panel b.

from the mid-Holocene to the Recent, with larger changes in the northern BoB.

5.2. Estimating salinity at the mid-Holocene and LGM relative to present

Seawater $\delta^{18}O$ alone is insufficient to constrain salinity changes

associated with monsoonal hydroclimate due to the confounding influence of geographic and temporal changes in temperature. We use existing, but sparse, temperature data from the northern BoB (KL 126), the Andaman (RC12-344), and the southern BoB (ODP 758) combined with the BoB $\delta^{18}O_{sw}$ - salinity relationship to transform the $\delta^{18}O$ data into salinity estimates. This provides a more direct indication of changes in rainfall and runoff and yields a

Table 2
Area average salinities and % change relative to modern. Modelling results (NEMO) illustrate the change in salinity and fresh water input (precipitation and runoff) required to achieve the reconstructed salinity estimates.

Region	Time period			NEMO sensitivity experiment at different multiplicative factor				
	Modern salinity (psu)	Early to mid-Holocene	LGM	CTL	CTL_X0	CTL_X0.5	CTL_X1.5	CTL_X2
Northern BoB	31.04	28.52 (−8.11)	33.91 (9.25)	31.74	36.42 (+14.74)	34.25 (+7.90)	29.65 (−6.58)	28.21 (−11.11)
Andaman Sea	32.65	28.78 (−11.87)	32.50 (−0.46)	32.87	35.52 (+8.06)	34.68 (+5.50)	31.08 (−5.46)	29.69 (−9.68)
Southern BoB	33.71	32.51 (−3.56)	35.37 (4.91)	34.06	35.34 (+3.12)	34.88 (+2.41)	33.12 (−2.75)	32.30 (−5.18)
N−S salinity gradient (average for the basins)	2.68	3.99	1.46	2.32	1.08	0.64	3.48	4.09
N−S salinity gradient between 20°N and 5°N	3.83	5.07	1.06	3.54	1.29	1.17	5.09	5.88

(Percentage change is shown in bracket; negative sign denote freshening).

variable that can be directly compared to recent model salinity estimates (Akhil et al., 2014; Benshila et al., 2014; Jana et al., 2015; Vinayachandran et al., 2013). Estimated salinities are derived and presented in Table 1 and summarized in Table 2 and Fig. 9. Beyond the assumptions discussed in Section 2.2, we assume that the sparse temperature data, available for only one core in each of the three regions, can be extrapolated to the other cores in these regions. Additional SST data from cores in these three regions would be useful in further constraining the salinity structure.

During the mid-Holocene the northern BoB was ~8% fresher, the Andaman 12% fresher and the southern BoB ~3.5% fresher compared to modern. In contrast, during the LGM, the northern BoB was ~9% more saline, the Andaman was unchanged and the southern BoB ~5% more saline compared to modern. The LGM high salinity in the BoB corroborates earlier findings of Cullen (1981). In contrast, the finding of fresher Holocene values contrasts with Cullen (1981) who found no change in Holocene salinity relative to modern. The north to south BoB salinity gradient today is 2.7 psμ. We estimate that this gradient increased to 3.9 psμ during the mid-Holocene and decreased to 1.5 psμ during the LGM. These results are broadly consistent with estimates of changes at the LGM and mid-Holocene BoB of Govil and Naidu (2011) and Rashid et al. (2007) and are interpreted as reflecting increased mid-Holocene and decreased LGM precipitation and runoff associated with summer monsoon circulation (Fig. 9b). These changes are also consistent with the mean effective moisture record of the Central Asia (Herzschuh, 2006) (Fig. 9c).

Freshening in the northern BoB and Andaman during early to mid-Holocene is consistent with increased monsoonal precipitation and differences in proximity to the outflow of major rivers into the BoB. During the LGM, both the northern and southern BoB regions became more saline while the Andaman was largely unchanged. We attribute this to increased isolation of Andaman basin during the LGM sea-level low stand, restricting the mixing of surface waters with the open northern and southern BoB. Shelf exposure, leading to increased proximity of the Andaman cores to the Irrawaddy and Salween freshwater sources may also be a factor. Recent modelling shows that Irrawaddy river input, even in the modern, is not fully transported to the southern Andaman Sea but remains somewhat isolated in the northern half of the Andaman Basin (Benshila et al., 2014).

We interpret the reduced LGM northern to southern BoB salinity gradient (1.5 psμ) to reflect decreased oceanic precipitation and/or runoff during the LGM. A positive feedback involving reduced stratification would also allow for increased vertical mixing (possibly more so in the north), further reducing the salinity gradient.

5.3. Combining proxy data and model simulations to estimate changes in freshwater input

Relative to modern, our model results indicate that the mid-Holocene proxy estimates from the northern and southern BoB can be replicated by a ~50% increase in freshwater flux into the BoB (equally distributed in oceanic precipitation and runoff). Similarly, the LGM proxy estimates from the northern and southern BoB can be replicated by an ~50% decrease in freshwater flux (Fig. 10). We consider these changes as conservative estimates as we do not account in our modelling framework for the role of wind changes on vertical mixing during these periods; increased mid-Holocene precipitation is, for instance, likely accompanied by increased wind intensity over the BoB which would result in reduction of mid-Holocene surface freshening through increased vertical mixing.

The model results cannot be combined with proxy data to

estimate changes in Andaman Sea fresh water flux for the LGM because exchange with the BoB is greatly reduced during sea level low stands; all model sensitivity experiments use modern bathymetry. Model results indicate that the mid-Holocene proxy estimates from the Andaman require over 2 times the precipitation and runoff relative to CTL (Table 2). This is significantly larger than that estimated for the BoB, suggesting the possibility that the locus of mid-Holocene precipitation may have shifted eastward. Future work, incorporating winds and precipitation from paleoclimate model intercomparison projet (PMIP) simulations (Braconnot et al., 2012) can be used to evaluate this possibility.

5.4. Deglacial $\delta^{18}O$ structure

Clear YD structure (depleted $\delta^{18}O$) is present in the mixed-layer and thermocline records from the Andaman and northern BoB records. We have not attempted to account for the impact of temperature change and so can only infer that a combination of colder and/or more saline waters is responsible for this signal. Reduced fresh water input is consistent with previous work in the Andaman Sea (Rashid et al., 2007) and BoB (Govil and Naidu, 2011; Kudrass et al., 2001).

The lack of YD structure in even the best resolved southern BoB record (ODP 758) does not necessarily indicate that a YD signal was not present in the surface waters at this latitude (5°N). While ODP 758 has a sufficiently high temporal sample resolution, bioturbation combined with a very low sedimentation rate (~2.2 cm/ka) may have prevented preservation of the signal in the sediment record. The transition from the LGM to Holocene appears more abrupt in the northern BoB and Andaman compared to the southern BoB. This may reflect the proximity of fresh water sources although the impact of lower sedimentation rates and, in some cases, lower sample resolution may also be factors in smoothing the abruptness of the LGM to Holocene transition in the southern BoB records.

6. Conclusions

The combination of new $\delta^{18}O$ records (mixed-layer, thermocline and bottom dwelling foraminifera) and records compiled from the literature yield an eleven site north to south transect spanning the LGM to Recent, including three sites in the northern BoB and four sites each in the Andaman Sea and Southern BoB. One core within each region has a paired SST record which we use in combination with a newly compiled $\delta^{18}O_{sw}$ -salinity relationship to estimate past changes in salinity across both time (LGM to Recent) and latitude (5°−20°N). The NEMO model is then used to quantify the changes in freshwater input necessary to replicate the observed salinity patterns. The major findings are summarised below.

1. Relative to modern, enhanced monsoon precipitation and runoff during early Holocene caused freshening in the northern BoB (8%, 2.5 psμ), the Andaman (12%; 3.8 psμ) and the southern BoB (3.5%, 1.2 psμ). This represents an ~50% increase in the northern BoB to southern BoB salinity gradient (2.7−4 psμ) relative to modern, likely leading to enhanced surface stratification during the mid-Holocene. Modelling results suggest that the BoB changes can be produced by increased freshwater input on the order of 50% relative to present whereas the Andaman requires significantly more (>100%).
2. Relative to modern, decreased monsoon precipitation and runoff during the LGM led to increased salinity in the northern BoB (9%, 2.9 psμ) and the southern BoB (4.9%, 1.6 psμ). This represents an ~46% decrease in the northern BoB to southern BoB salinity gradient (2.7−1.5 psμ) relative to modern, likely

leading to reduced surface stratification during the LGM. Modelling results for the BoB suggest that these changes can be produced by decreased freshwater input in the order of 50% relative to modern.

3. Relative to modern, Andaman salinity during the LGM was largely unchanged. Noting the increased salinity of the northern and southern BoB regions, one might expect reduced LGM precipitation and runoff in the Andaman as well. We attribute the Andaman results to reduced mixing of surface waters with open northern and southern BoB waters, driven by increased isolation of the basin during the sea-level low stand or to emergence of the shelf (increasing the proximity of the core sites to the river mouths).

4. Clear YD structure is observed in the northern BoB and Andaman Sea records (both mixed-layer and thermocline-dwelling species) indicating cooling and/or reduced fresh water input. YD structure is not resolved in the southern BoB records. However, noting the resolved LGM and mid-Holocene signals in the southern BoB records, a YD signal may have been present in the surface waters but not recorded in the sediment record due to the combined effects of bioturbation and low sedimentation rates.

Acknowledgements

Appendix A. Supplementary data

Supplementary data related to this article can be found at http://dx.doi.org/10.1016/j.quascirev.2016.01.022.

References

Achyuthan, H., Deshpande, R.D., Rao, M.S., Kumar, B., Nallathambi, T., Kumar, K.S., Ramesh, R., Ramachandran, P., Maurya, A.S., Gupta, S.K., 2013. Stable isotopes and salinity in the surface waters of the Bay of Bengal: implications for water dynamics and palaeoclimate. Mar. Chem. 149, 51−62.

Ahmad, S.M., Babu, G.A., Padmakumari, V.M., Raza, W., 2008. Surface and deep water changes in the northeast Indian Ocean during the last 60 ka inferred from carbon and oxygen isotopes of planktonic and benthic foraminifera. Palaeogeogr. Palaeoclimatol. Palaeoecol. 262, 182−188.

Ahmad, S.M., Patil, D.J., Rao, P.S., Nath, B.N., Rao, B.R., Rajagopalan, G., 2000. Glacial-interglacial changes in the surface water characteristics of the Andaman Sea: evidence from stable isotopic ratios of planktonic foraminifera. Proc. Indian Acad. Sci. (Earth Planet. Sci.) 109, 153−156.

Akhil, V.P., Durand, F., Lengaigne, M., Vialard, J., Keethi, M.G., Gopalakrishna, V.V., Deltel, C., Papa, F., de Boyer Montégut, C., 2014. A modeling study of the processes of surface salinity seasonal cycle in the Bay of Bengal. J. Geophys. Res. 116, 3926−3947. http://dx.doi.org/10.1002/2013JC009632.

Ali, S., Hathorne, E.C., Frank, M., Gebregiorgis, D., Stattegger, K., Stumpf, R., Kutterolf, S., Johnson, J.E., Giosan, L., 2015. South Asian monsoon history over the past 60 kyr recorded by radiogenic isotopes and clay mineral assemblages in the Andaman Sea. Geochem. Geophys. Geosyst. 16 http://dx.doi.org/10.1002/2014GC005586.

Anand, P., Elderfield, H., Conte, M.H., 2003. Calibration of Mg/Ca thermometry in planktonic foraminifera from a sediment trap time series. Paleoceanography 18, 1050. http://dx.doi.org/10.1029/2002PA000846.

Antonov, J.I., Seidov, D., Boyer, T.P., Locarnini, R.A., Mishonov, A.V., Garcia, H.E., Baranova, O.K., Zweng, M.M., Johnson, D.R., 2010. World ocean atlas 2009. In: Salinity, vol. 2. U.S. Government Printing Office, Washington, D.C, p. 184. NOAA Atlas NESDIS 69.

Awasthi, N., Ray, J.S., Singh, A.K., Band, S.T., Rai, V.K., 2014. Provenance of the Late Quaternary sediments in the Andaman Sea: implications for monsoon variability and ocean circulation. Geochem. Geophys. Geosyst. 15, 3890−3906.

Belanger, P.E., Curry, W.B., Matthews, R.K., 1981. Core-top evaluation of benthic foraminiferal isotopic ratios for paleo-oceanographic interpretations. Palaeogeogr. Palaeoclimatol. Palaeoecol. 33, 205−220.

Benshila, R., Durand, F., Masson, S., Bourdallé-Badie, R., de Boyer Montégut, C., Papa, F., Madec, G., 2014. The upper Bay of Bengal salinity structure in a high-resolution model. Ocean. Model. 74, 36−52.

Bolton, C.T., Chang, L., Clemens, S.C., Kodama, K., Ikehara, M., Medina-Elizalde, M., Paterson, G.A., Roberts, A.P., Rohling, E.J., Yamamoto, Y., Zhao, X., 2013. A 500,000 year record of Indian summer monsoon dynamics recorded by eastern equatorial Indian Ocean upper water-column structure. Quat. Sci. Rev. 77, 167−180.

Braconnot, P., Harrison, S.P., Kageyama, M., Bartlein, P.J., Delmotte, V.M., Ouchi, A.A., Otto-Bliesner, B., Zhao, Y., 2012. Evaluation of climate models using palaeoclimatic data. Nat. Clim. Change 2 (6), 417−424.

Chaitanya, A.V.S., Lengaigne, M., Vialard, J., Gopalakrishna, V.V., Durand, F., KranthiKumar, C., Amrithash, S., Suneel, V., Papa, F., Ravichandran, M., 2014. Fishermen-operated Salinity Measurements Reveal a "River in the Sea" Flowing Along the East Coast of India. BAMS online first. http://dx.doi.org/10.1175/BAMS-D-12-00243.1.

Chen, J., 1994. Benthic Foraminiferal Isotopic Composition: Implications for Late Neogene-Quaternary Paleoceanography of the Indian Ocean. Ph.D. Thesis. Brown University.

Chen, M.−T., Farrell, J.W., 1991. Planktonic foraminifer faunal variations in the northeastern Indian Ocean: a high-resolution record of the past 800,000 years from Site 758. In: Weissel, J., Peirce, J., Taylor, E., et al. (Eds.), Proceedings of the Ocean Drilling Program, Scientific Results, College Station, TX (Ocean Drilling Program), 121, pp. 125−140. http://dx.doi.org/10.2973/odp.proc.sr.121.174.1991.

Colin, C., Kissel, C., Blamart, D., Turpin, L., 1998. Magnetic properties of sediments in the Bay of Bengal and the Andaman Sea: impact of rapid North Atlantic Ocean climatic events on the strength of the Indian monsoon. Earth Planet Sci. Lett. 160, 623−635.

Colin, C., Turoin, L., Bertaux, J., Desprairies, A., Kissel, C., 1999. Erosional history of the Himalayan and Burman ranges during the last two glacial-interglacial cycles. Earth Planet. Sci. Lett. 171, 647−660.

Colin, C., Turpin, L., Blamart, D., Frank, N., Kissel, C., Duchamp, S., 2006. Evolution of weathering patterns in the Indo-Burman ranges over the last 280 kyr: effects of sediment provenance on $^{87}Sr/^{86}Sr$ ratios tracer. Geochem. Geophys. Geosyst. 7, Q03007. http://dx.doi.org/10.1029/2005GC000962.

Cullen, J., 1981. Microfossil evidence for changing salinity patterns in the Bay of Bengal over the last 20,000 years. Palaeogeogr. Palaeoclimatol. Palaeoecol. 35, 315−356.

Dee, D.P., et al., 2011. The ERA-interim reanalysis: configuration and performance of the data assimilation system. Q. J. R. Meteorol. Soc. 137, 553−597. http://dx.doi.org/10.1002/qj.828.

Delaygue, G., Bard, E., Rollion, C., Jouzel, J., Stievenard, M., Duplessy, J.C., Ganssen, G., 2001. Oxygen isotope/salinity relationship in the northern Indian Ocean. J. Geophys. Res. 106 (C3), 4565−4574.

Duplessy, J.−C., 1982. Glacial to interglacial contrasts in the northern Indian Ocean. Nature 295, 494−498.

Duplessy, J.−C., 1996. Quaternary paleoceanography: unpublished stable isotope records. In: IGBP PAGES/World Data Center for Paleoclimatology Data Contribution Series #1996-035. NOAA/NGDC Paleoclimatology Program, Boulder, Colorado, USA.

Dussin, R., Barnier, B., Brodeau, L., 2014. Atmospheric Forcing Data Sets to Drive Eddy-resolving Global Ocean General Circulation Models (EGU General Assembly Conference Abstracts).

Fekete, B.M., Vorosmarty, C.J., Grabs, W., 2002. High-resolution fields of global runoff combining observed river discharge and simulated water balances. Glob. Biogeochem. Cycles 16 (3), 1042. http://dx.doi.org/10.1029/1999GB001254.

Gauns, M., Madhupratap, M., Ramaiah, N., Jyothibabu, R., Fernandes, V., Paul, J.T., Prasanna Kumar, S., 2005. Comparative accounts of biological productivity characteristics and estimates of carbon fluxes in the Arabian Sea and the Bay of Bengal. Deep Sea Res. 52, 2003−2017.

Govil, P., Naidu, P.D., 2011. Variations of Indian monsoon precipitation during the last 32 kyr reflected in the surface hydrography of the Western Bay of Bengal. Quat. Sci. Rev. 30, 3871−3879.

Herzschuh, U., 2006. Palaeo-moisture evolution in monsoonal Central Asia during the last 50,000 years. Quat. Sci. Rev. 25, 163−178.

Huffman, G.J., Adler, R.F., Morrissey, M.M., Curtis, S., Joyce, R., McGavock, B., Susskind, J., 2001. Global precipitation at one-degree daily resolution from multi-satellite observations. J. Hydrom. 2, 36−50.

Jana, S., Gangopadhyay, A., Chakraborty, A., 2015. Impact of seasonal river input on the Bay of Bengal simulation. Cont. Shelf Res. 104, 45—62.

Kudrass, H.R., Hofmann, A., Doose, H., Emeis, K., Erlenkeuser, H., 2001. Modulation and amplification of climatic changes in the Northern Hemisphere by the Indian summer monsoon during the past 80 k.y. Geology 29, 63—66.

Kurian, S., Nath, B.N., Ramaswamy, V., Naman, D., Rao, T.G., Kamesh Raju, K.A., Selvaraj, K., Chen, C.T.A., 2008. Possible detrital, diagenetic and hydrothermal sources for Holocene sediments of the Andaman backarc basin. Mar. Geol. 247, 178—193.

Leduc, G., Sachs, J.P., Kawka, O.E., Schneider, R.R., 2013. Holocene changes in eastern equatorial Atlantic salinity as estimated by water isotopologues. Earth Planet. Sci. Lett. 362, 151—162.

LeGrande, A.N., Schmidt, G.A., 2006. Global gridded data set of the oxygen isotopic composition in seawater. Geophys. Res. Lett. 33, L12604. http://dx.doi.org/10.1029/2006GL026011.

Levitus, S., Boyer, T., 1994. World ocean atlas 1994. In: Temperature, vol. 4. US Department of Commerce, Washington, DC, p. 99.

Lisiecki, L.E., Raymo, M.E., 2005. A pliocene-pleistocene stack of 57 globally distributed benthic delta ^{18}O records. Paleoceanography 20, PA1003. http://dx.doi.org/10.1029/2004PA001071.

Locarnini, R.A., Mishonov, A.V., Antonov, J.I., Boyer, T.P., Garcia, H.E., Baranova, O.K., Zweng, M.M., Johnson, D.R., 2010. World ocean atlas 2009. In: Levitus, S. (Ed.), Temperature, vol. 1. Government Printing Office, Washington, D.C, p. 184. NOAA Atlas NESDIS 68.

Madec, G., 2008. NEMO, the ocean engine. In: Note du Pole de Model., 27, Inst. Pierre-Simon Laplace, Paris. Available at: http://www.nemo-ocean.eu/About-NEMO/Reference-manuals.

Marchesiello, P., McWilliams, J.C., Shchepetkin, A., 2001. Open boundary conditions for long-term integration of regional ocean models. Ocean. Model. 3, 1—20.

Marzin, C., Kallel, N., Kageyama, M., Duplessy, J.-C., Braconnot, P., 2013. Glacial fluctuations of the Indian monsoon and their relationship with North Atlantic climate: new data and modelling experiments. Clim. Past. 9, 2135—2151.

Mohtadi, M., Oppo, D.W., Lückge, A., DePol-Holz, R., Steinke, S., Groeneveld, J., Hemme, N., Hebbeln, D., 2011. Reconstructing the thermal structure of the upper ocean: insights from planktic foraminifera shell chemistry and alkenones in modern sediments of the tropical eastern Indian Ocean. Paleoceanography 26, PA3219. http://dx.doi.org/10.1029/2011PA002132.

Naqvi, W.A., Charles, C.D., Fairbanks, R.G., 1994. Carbon and oxygen isotopic records of benthic foraminifera from the Northeast Indian Ocean: implications on glacial-interglacial atmospheric CO_2 changes. Earth Planet. Sci. Lett. 121, 99—110.

Neetu, S., Lengaigne, M., Vincent, E.M., Vialard, J., Madec, G., Samson, G., Ramesh Kumar, M.R., Durand, F., 2012. Influence of upper-ocean stratification on tropical cyclone-induced surface cooling in the Bay of Bengal. J. Geophys. Res. 117, C12020. http://dx.doi.org/10.1029/2012JC008433.

Papa, F., Bala, S.K., Pandey, R.K., Durand, F., Gopalakrishna, V.V., Rahman, A., Rossow, W.B., 2012. Ganga—Brahmaputra river discharge from Jason-2 radar altimetry: an update to the long-term satellite-derived estimates of continental freshwater forcing flux into the Bay of Bengal. J. Geophys. Res. 117, C11021. http://dx.doi.org/10.1029/2012JC008158.

Prasanna Kumar, S., Muraleedharan, P.M., Prasad, T.G., Gauns, M., Ramaiah, N., De Souza, S.N., Sardesai, S., Madhupratap, M., 2002. Why is the Bay of Bengal less productive during summer monsoon compared to the Arabian Sea? Geophys. Res. Lett. 29, 2235. http://dx.doi.org/10.1029/2002GL016013.

Ramprasad, T., Dewangan, P., Ramana, M.V., Mazumdar, A., Karisiddaiah, S.M., Ramya, E.R., Sriram, G., 2011. Evidence of slumping/sliding in Krishna-Godavari offshore basin due to gas/fluid movements. Mar. Pet. Geol. 28, 1806—1816.

Rao, R.R., Sivakumar, R., 2003. Seasonal variability of sea surface salinity and salt budget of the mixed layer of the north Indian Ocean. J. Geophys. Res. 108 (C1), 3009. http://dx.doi.org/10.1029/2001JC000907.

Rashid, H., Flower, B.P., Poore, R.Z., Quinn, T.M., 2007. A ~25 ka Indian Ocean monsoon variability record from the Andaman Sea. Quat. Sci. Rev. 26, 2586—2597.

Ravelo, A.C., Fairbanks, R.G., Philander, S.G.H., 1990. Reconstructing tropical Atlantic hydrography using planktonic foraminifera and ocean model. Paleoceanography 5, 409—431.

Raza, T., Ahmad, S.M., Sahoo, M., Banerjee, B., Bal, I., Dash, S., Suseela, G., Mukherjee, I., 2014. Hydrographic changes in the southern Bay of Bengal during the last ~65,000 y inferred from carbon and oxygen isotopes of foraminiferal fossil shells. Quatern. Int. 333, 77—85.

Sarma, V.V.S.S., Narvekar, P.V., 2001. A study on inorganic carbon components in the Andaman Sea during the post monsoon season. Oceanol. Acta 24, 125—134.

Schmidt, G.A., 1999. Error analysis of paleosalinity calculations. Paleoceanography 14, 422—429.

Schmidt, G.A., Bigg, G.R., Rohling, E.J., 1999. Global Seawater Oxygen-18 Database, vo1. 21. http://data.giss.nasa.gov/o18data/.

Sengupta, D., Bharath Raj, G.N., Shenoi, S.S.C., 2006. Surface freshwater from Bay of Bengal runoff and Indonesian throughflow in the tropical Indian Ocean. Geophys. Res. Lett. 33, L22609. http://dx.doi.org/10.1029/2006GL027573.

Sengupta, S., Parekh, A., Chakraborty, S., Kumar, K.R., Bose, T., 2013. Vertical variation of oxygen isotope in Bay of Bengal and its relationships with water masses. J. Geophys. Res. Oceans 118, 6411—6424. http://dx.doi.org/10.1002/2013JC008973.

Shackleton, N.J., Hall, M.A., 1984. Oxygen and Carbon Isotope Stratigraphy of Deep Sea Drilling Project Hole 552A: Plio-pleistocene Glacial History, pp. 599—609. Initial Reports of the Deep Sea Drilling Project.

Shenoi, S.S.C., Shankar, D., Shetye, S.R., 2002. Difference in heat budgets of the near-surface Arabian Sea and Bay of Bengal: implications for the summer monsoon. J. Geophys. Res. 107 (C6), 3052. http://dx.doi.org/10.1029/2000JC000679.

Sijinkumar, A.V., Nath, B.N., Guptha, M.V.S., 2010. Late Quaternary record of pteropods preservation from the Andaman Sea. Mar. Geol. 275, 221—229. http://dx.doi.org/10.1016/j.margeo.2010.06.003.

Sijinkumar, A.V., Nath, B.N., Possnert, G., Aldahan, A., 2011. Pulleniatina minimum events in the Andaman Sea (NE Indian Ocean): implications for winter monsoon and thermocline changes. Mar. Micropaleontol. 81, 88—94. http://dx.doi.org/10.1016/j.marmicro.2011.09.001.

Sijinkumar, A.V., Nath, B.N., Guptha, M.V.S., Ahmad, S.M., Rao, B.R., 2015. Timing and preservation mechanism of deglacial pteropods spike from the Andaman Sea, northeastern Indian Ocean. Boreas 44, 432—444.

Singh, A., Jani, R.A., Ramesh, R., 2010. Spatiotemporal variations of the δ^{18}O-salinity relation in the northern Indian Ocean. Deep Sea Res. I 57, 1422—1431.

Vinayachandran, P.N., Shankar, D., Vernekar, S., Sandeep, K.K., Amol, P., Neema, C.P., Chatterjee, A., 2013. A summer monsoon pump to keep the Bay of Bengal salty. Geophys. Res. Lett. 40, 1777—1782.

Zhang, Y., Rossow, W.B., Lacis, A.A., Oinas, V., Mishchenko, M.I., 2004. Calculation of radiative fluxes from the surface to top of atmosphere based on ISCCP and other global data sets: refinements of the radiative transfer model and the input data. J. Geophys. Res. 109, D19105. http://dx.doi.org/10.1029/2003JD004457.